Proceedings of the 21st ICSMGE, Vienna, Austria, 14 – 19 June 2026. Pistrol, Adam & Schweiger (eds.)
Published by: ÖGG, Austrian Society for Geomechanics, Salzburg, Austria, ISBN 978-3-9503898-4-5
https://doi.org/10.53243/ICSMGE2026-1232

An experimental investigation on the performance of shared suction anchors under multi-directional loading in clay

Ying Huang
Southeast University, Nanjing, China, yinghuang@seu.edu.cn

Jianbin Cui
Southeast University, Nanjing, China

Chuheng Wu
Southeast University, Nanjing, China

Youhu Zhang
Southeast University, Nanjing, China

ABSTRACT: Shared anchoring emerges as a promising technology for reducing the cost of floating offshore wind as it can drastically reduce the number of anchors. However, by connecting multiple mooring lines to an anchor, shared anchors are subject to multi-directional loading conditions that differ significantly from conventional single line anchors, especially during typhoon events. This necessitates research into the bearing characteristics of shared anchor in order to develop design methodologies. In this paper, an experimental study on the performance of shared suction anchors in clay is reported. A series of physical model tests of suction anchors under multi-directional loading are carried out. The multi-directional loading is realized by two orthogonal loading axes which are controlled independently. The results indicate that the performance of shard anchors is highly dependent on the resultant load inclination angle, for both monotonic and cyclic loading conditions. The multi-directional loading effects due to typhoon passage influence the anchor performance by altering the resultant load inclination angle in essence. It is recommended that the most critical resultant load inclination angle should be considered in design and the padeye depth should be determined accordingly.

KEYWORDS: Floating offshore wind; shared suction anchor; multi-directional loading; clay; physical model testing.

1 INTRODUCTION

Suction anchors are recognized for their convenient installation and economic efficiency in deep waters (Andersen and Jostad, 1999; Fu et al., 2020). With the development of floating offshore wind industry, suction anchors have been a popular anchoring solution for securing floating wind turbines (e.g., Hywind Scotland, Hywind Tampen, Three Gorges Pioneer, CNOOC Guanlan). In recent years, shared anchoring emerges as a promising technology for reducing the cost of floating offshore wind as it can drastically reduce the number of anchors (Diaz et al., 2016; Fontana et al., 2018). This concept was first implemented in the Hywind Tampen project, located approximately 140 km offshore in the Norwegian North Sea. In this project, a total of 19 suction anchors were installed to moor 11 floating wind turbines, corresponding to a 42% reduction in anchor requirements relative to the Hywind Scotland project. However, by connecting multiple mooring lines to an anchor, shared anchors are subject to multi-directional loading conditions that differ significantly from conventional single line anchors, which garners increasing attention from researchers (Fontana, 2019; Barron et al., 2024; Barron et al., 2025).

Fontana (2019) systematically examined the loading conditions of shared anchors by numerical simulation. It is revealed that in contrast to a single line anchor whose line tension is always along the mooring line, the resultant loading direction of a shared anchor is aligned with the environmental loading direction, although an angular range about 30° is observed due to phase differences between the mooring lines. This suggests that during typhoon condition, a shared anchor will experience cyclic loading whose resultant direction varies over time. This reflects the temporal evolution of wind and wave directions throughout the event. (Li et al., 2018; Li et al., 2023).

According to DNV-ST-0119 (DNV, 2021), particular attention should be given to the complex loading effects generated by the multiple mooring lines. However, specific design guidelines and methodologies remain absent. Chung (2012) demonstrated negative effects of multi-directional loading on both pile and suction anchors in clay. However, due to equipment limitations related to the complexity of orthogonal loading synchronization, the findings fail to reflect the multiple mooring conditions and have restricted applicability to design. Recently, several studies have further highlighted the multidirectional effects on shared foundations (e.g., pile anchors, ring anchors, suction anchors in sand), and corresponding design framework were proposed (Yan et al., 2024; Abadie, 2025; Huang et al., 2025). However, both the detailed mechanisms and design recommendations for shared suction anchors under multi-directional loading in clay have not yet been clarified. The relevant research remains an emerging area.

In an attempt to fill the knowledge gap, an experimental study on the performance of shared suction anchors in clay is reported in this paper. A series of physical model tests of suction anchors under loading conditions relevant to shared anchoring are carried out. Multi-directional loading effects, considering continuous evolution of resultant loading direction under typhoon passage are examined. The primary objective of the study is to identify the potential risks and to assess their impact to anchor performance. Implications to design of shared suction anchors in clay are discussed.

2 SET-UP OF THE PHYSICAL MODEL TESTING

2.1 *Model anchor geometry*

The model suction is fabricated from 7075 aluminum, as shown in Figure 1 (a) ~ (b). The dimensions of the model suction and prototype suction are listed in Table 1, assuming a

scaling ratio of 1:60. Due to the fabrication constraint, the diameter to wall thickness ratio used in model testing is smaller than that typically employed in practice. However, this is not anticipated to significantly impact on the anchor's behaviour. The model anchor is welded with two orthogonally-positioned padeyes, supplied with 4 mm high-strength steel wire ropes as shown in Figure 1 (a). Padeyes are located at 2/3L (L is the embedment length) below mudline, which are deliberately designed to be lower than the optimum depth for the undrained shear strength profile and loading angle considered in the current experiments to avoid gap formation as recommended by Andersen and Jostad (1999). In addition, two drainage valves are mounted on the top of the anchor for evacuation of air and water during anchor installation, as shown in Figure 1 (b).

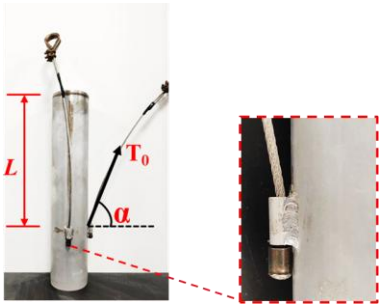

(a) The side view of model anchor

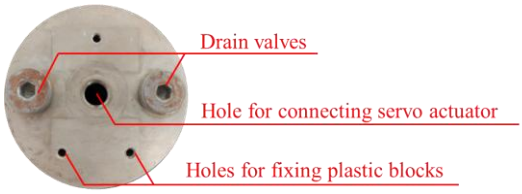

(b) The top view of model anchor

Figure 1. Model suction anchor used for testing.

2.2 *Load application*

A simplified orthogonal loading model system is used in this study to simulate the loading condition of the practical shared anchor, as shown in Figure 2 (a) and (b). The system includes two vertical reaction frames, high strength and low friction pulley systems, and two electrical servo actuators. To track the six-degree-of-freedom motion of the anchor, three LVDT sensors with ball connections at both ends and a 3D inclinometer are attached to the anchor through a light weight plastic block. Assuming the anchor behaves as a rigid body, the motions at the padeye can be easily derived from the measured displacements and rotations.

Figure 3 shows the relation between the resultant load F_R, and the two orthogonal mooring line tensions. The relationship can be described by Equations (1) ~ (3).

$$F_{\mathrm{R}} = F_{\mathrm{Y}} / (1+\tan^2\beta + 2\tan\beta\cdot\sin^2\alpha)^{-0.5} \quad (1)$$

$$\beta = \arctan(F_X / F_{\mathrm{Y}}) \quad (2)$$

$$\alpha_{\mathrm{R}} = \arctan\left(\frac{\tan\alpha\cdot(1+\tan\beta)}{(1+\tan^2\beta)^{0.5}}\right) \quad (3)$$

where F_{X} and F_{Y} represent the inclined tension forces in orthogonal mooring lines; α is the inclination angle of the mooring line with the horizontal plane at the padeye, which is set to 30° for both mooring lines in the current experiments; α_{R} and β stands for inclination angle with the horizontal plane and direction from the Y axis of the resultant load, respectively, as illustrated by Figure 3.

The two orthogonal loading axes are programmed to run in synchronization in either load or displacement control. This allows simulation of the testing loading conditions that are relevant for shared suction anchors, as illustrated by Figure 4: continuous evolution of resultant loading direction, mimicking the conditions during typhoon passage.

Based on experience, the cyclic to average load ratio ($F_{\mathrm{cy}}/F_{\mathrm{a}}$) as defined in Figure 4 was set to 0.6 and the loading frequency was set 0.1 Hz in the current experiments.

Table 1. Summary of anchor dimensions.

Parameter	Unit	Model	Prototype
Diameter, D	m	0.08	4.8
Wall thickness, t	m	0.002	0.03
Embedment length, L	m	0.4	24
Young's modulus, E	GPa	71.7	210

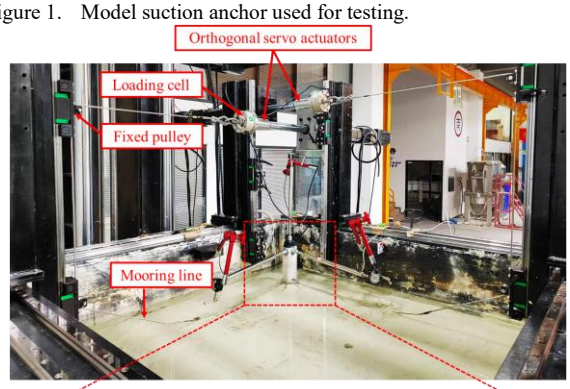

(a) Loading device

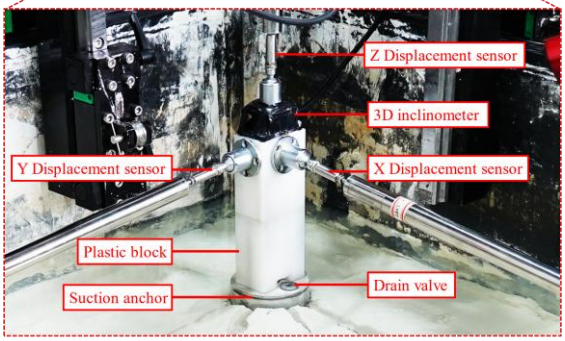

(b) Monitoring system

Figure 2. Loading set-up and monitoring system for model tests.

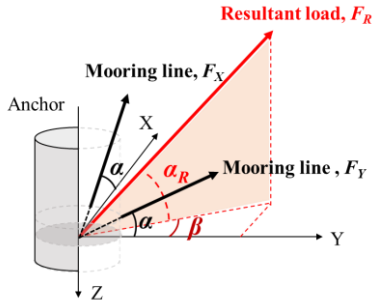

Figure 3. Relationship between the resultant load and tensions from two orthogonal mooring line tensions.

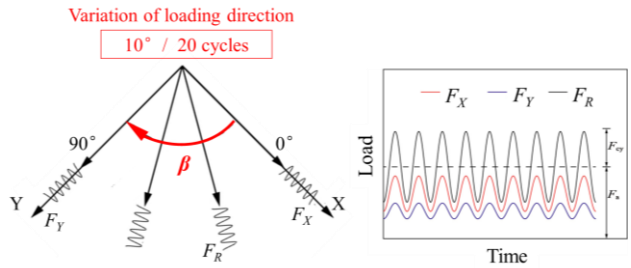

Figure 4. Loading conditions applied in model tests.

2.3 *Soil sample preparation*

One soil sample was prepared from Malaysian kaolin, which is commonly employed in geotechnical model testing. The clay has a d_{60} of 0.006mm and a plasticity index of 24.5% (the plastic and liquid limit are 37.5% and 62.0%, respectively).

The soil sample preparation process is illustrated by Figure 5 (a). The soil sample was prepared in a square container, which measures 1.2m x 1.2m in plan and 1.25m in height. Slurry with a water content of 130% was firstly produced by mixing kaolin powder with water in a mixer. The slurry was then transferred to the container and incrementally consolidated under a hydraulic press to a final pressure of 55 kPa. The settlement of the sample was monitored by a LVDT.

To facilitate drainage during consolidation, a 100 mm layer of gravel drainage layer was placed at the base of container and the drainage valves located at the bottom of the container were maintained open. The side walls of the container were coated with a layer of Vaseline. The top plate through which the consolidation stress is applied was perforated with 10 mm diameters holes and wrapped with geotextile to facilitate drainage. The hydraulic consolidation pressure was released after completion of consolidation and time was allowed for the soil to swell before testing.

Figure 5 (b) presents the undrained shear strength profile of the soil sample measured by T-bar penetrometer (25.2mm in diameter and 126.1mm in length) and a miniature vane shear apparatus. Results demonstrate good match between the T-bar test and the vane shear tests. The T-bar was conducted at a penetration velocity of 1 mm/s, ensuring undrained penetration process. The undrained shear strength profile was derived with a $N_{T\text{-}bar}$ factor of 10.5. Shallow correction as proposed by White et al. (2010) was performed for depths where a localized flow-around mechanism was not yet formed.

2.4 *Testing procedures and test programme*

The model anchor was jacked to target depth at a constant velocity of 1mm/s. Drainage values were kept open during installation and were closed before loading. After installation, the anchor was left undisturbed for 8 hours to allow pore pressure dissipation, which was sufficient to achieve 90% dissipation.

In total, six tests were performed in this study as summarized in Table 2. Two monotonic tests were conducted to investigate the differences in failure modes between the shared anchor and traditional single line anchor. The other four cyclic tests aimed to investigate the performance of shared anchor under multi-directional loading conditions.

(a) Soil sample preparation process

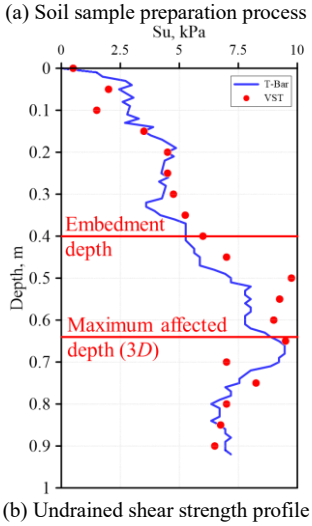

(b) Undrained shear strength profile

Figure 5. Soil sample preparation produre and soil strength profile.

Table 2. Testing programme in detail.

Test	Operation	Load conditions
Mono_1	Single line anchor, $\alpha = 30°$	$v = 36$ mm/min.
Mono_2	Single line anchor, $\alpha = 40°$ (Simulating the shared anchor with a fixed direction, $\alpha_R = 40°$)	$v = 56.93$ mm/min for resultant.
Cyclic_1	Single line anchor, $\alpha = 30°$.	$F_{max} = 40\%\ F_u$. $N = 200$.
Cyclic_2	Shared anchor, $\alpha = 30°$. Resultant loading direction (β) is 45° (fixed mean direction, $\alpha_R \approx 40°$).	$F_{max} = 40\%\ F_u$. $N = 200$.
Cyclic_3	Shared anchor, $\alpha = 30°$. Resultant loading direction (β) is rotated by 10° every 20 cycles, covering the range from 0° to 90°.	$F_{max} = 40\%\ F_u$. $N = 200$.

Note: F_u is the ultimate capacity obtained from test Mono_1; F_{max} is the maximum resultant load during cyclic loading, and N is the total number of cycles.

According to the drainage criteria proposed by Finnie and Randolph (1994), monotonic tests were performed in displacement control with a constant mooring line pulling velocity of 0.6 mm/s. Cyclic tests were performed in load control model. The loss in line tension caused by friction at the fixed pulley was checked by comparison of loads measured at the end of the actuator and immediately above the mudline as

shown in Figure 6 (a). Results presented in Figure 6 (b) suggest that fictional loss is small for loads less than 1 kN.

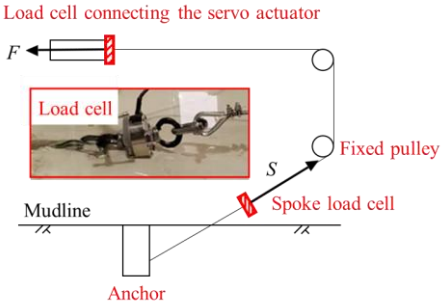

(a) Monitoring of line tension applied to the anchor.

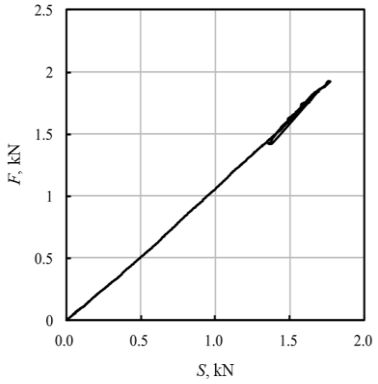

(b) Comparison of loads measured by two load cells.

Figure 6. Verification for system frictional loss.

3 MODEL TEST RESULTS

3.1 *Effect of resultant loading angle (α_R) due to multi-directional loading*

As captured by Eq. (3), when the shared suction anchor is loaded simultaneously in X and Y axes, the inclination angle of the resultant load to the horizontal plane (α_R) is different from the angle of individual load component (α). When α is 30° and β=45° (i.e., the same loading amplitude in X and Y axes), Eq. (3) gives α_R=39.2°. To investigate the difference in performances between single-line anchor and shared anchor under monotonic loading, Tests Mono_1 and Mono_2 were performed. In Mono_2, although the load was applied through a single mooring line, the effect of multi-directional loading is considered by increasing the mooring line inclination angle from 30° to 40°.

Figure 7 presents comparison of the results from the two tests. As shown in Figure 7 (a), it is clear that the holding capacity of the anchor is dependent on the resultant inclination angle. The ultimate holding capacity is approximately 840 N and 667 N for anchor with α_R = 30° and 40°, respectively.

In Figure 7 (b), the load-displacement curves are compared for the vertical and the horizontal components. It is noticed that, the horizontal bearing capacity and stiffness of the anchor with α_R = 30° are significantly higher than those with α_R = 40° due to mobilization of a considerably larger soil wedge. In contrast, a similar ultimate vertical capacity was observed in both tests.

In this study, the sudden loss of suction behind the anchor in Test Mono_1 caused a steep drop in capacity after the peak.

In essence, when the shared anchor is subject to mooring line tension from multiple loading directions, the resultant load inclination angle (α_R) is increased while the depth of equivalent loading point at the anchor centerline (Z_{cl}) remains unchanged, as illustrated in Figure 8. The holding capacity of shared suction anchor is significantly influenced by α_R.

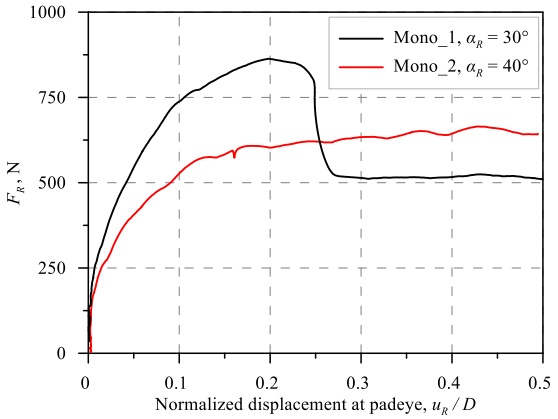

(a) Resultant load-displacement responses

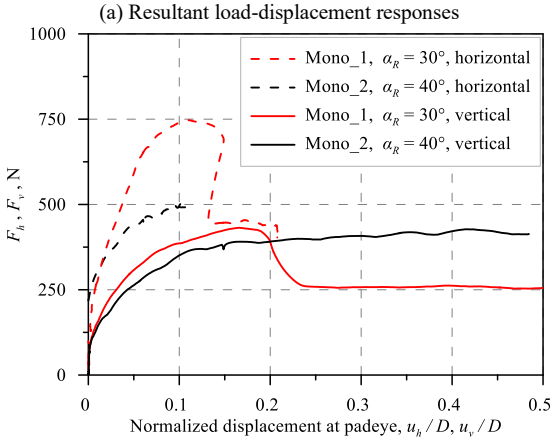

(b) Vertical and horizontal load-displacement responses

Figure 7. Comparison of response under monotonic loading between single line anchor and shared anchor.

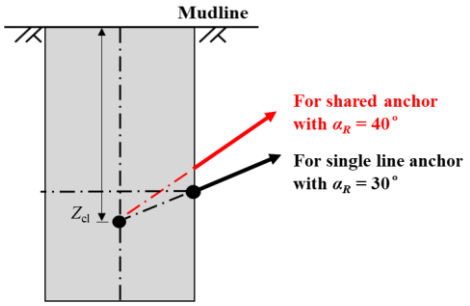

Figure 8. Differences in loading mode between single line anchor and shared anchor.

The impact of α_R on the performance of suction anchor is also found in the cyclic tests. Tests Cyclic_1 and Cyclic 2 have the same resultant load amplitude (F_{max}/F_u=0.4) and the same number of cycles (N=200). Test Cyclic_1 is loaded by one mooring line with α_R=30° while Test Cyclic_2 is loaded by two mooring lines with α_R≈40° as illustrated in Figure 5. The load-displacement results of these two tests, together with results of their monotonic reference tests, are presented in Figure 9 (a).

The cyclic tests exhibit close agreement with the monotonic reference tests during the first cycle, demonstrating excellent repeatability. Under cyclic loading, the suction anchor loaded by two lines exhibits much faster displacement accumulation than the anchor loaded by a single line. The corresponding displacement components are shown in Figure 9 (b). It is clear that for the shared anchor, the change of α_R drastically accelerates the development of vertical displacement under cyclic loading.

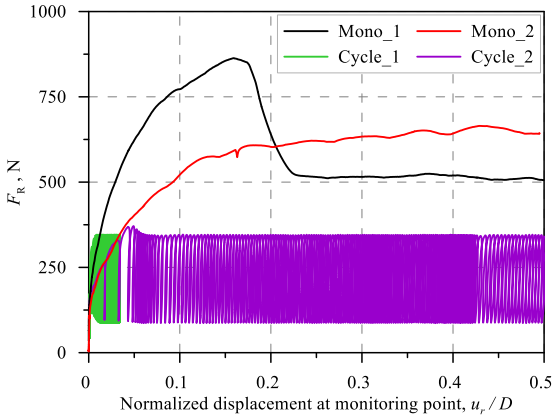

(a) Resultant displacement response

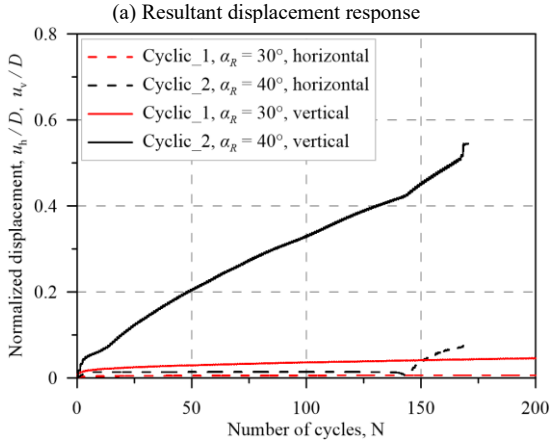

(b) Component displacement response

Figure 9. Comparisions of response under cyclic loading with fixed loading direction between singe line anchor and shared anchor.

3.2 *Effect of evolution of resultant loading direction with time under typhoon*

Figure 10 (a) present the load histories applied in the X and Y axes as well as the resultant loads in Test Cyclic_3. The test is divided into 10 loading episodes, within each 20 cycles are applied and the loading direction is kept constant. By varying the relative load magnitudes on the two orthogonal mooring lines in different loading episodes, the maximum resultant load is maintained constant while the resultant direction (β) changes over time from 0° to 90°. Figure 10 (b) presents the load-displacement curves of Test Cyclic_3. The displacement accumulation rate is shown to vary in synchronization with β. When β is 0° or 90°, the accumulation rate is low. However, when β=40-50°, the accumulation rate is high and the maximum accumulation rate is obtained.

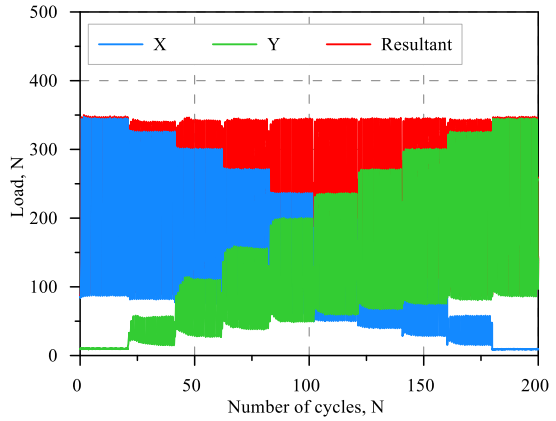

(a) Load histories as β changes from 0° to 90°

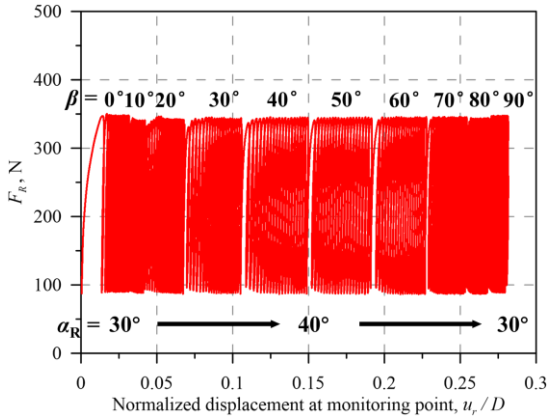

(b) Load-displacement curves as β changes from 0° to 90°

Figure 10. Testing results of Cyclic_3.

In Test Cyclic_3, the resultant loading direction rotates progressively over 90° and one may expect that the domain of soil is mobilized by the anchor rotates. However, the dominant factor in anchor performance seems to still lie in the change of α_R during this process (varying from 30° to 40° and then returns to 30°), as calculated by Equations (1) ~ (3). The influences of the change of α_R should be given particular attention in practical design.

4 CONCLUSIONS AND IMPLICATIONS FOR DESIGN

Shared anchoring emerges as a promising technology for cutting down the cost of mooring systems for floating offshore wind. Although the DNV-ST-0119 standard (DNV, 2021) clearly emphasize the need to consider the complex loading conditions of shared anchors in design, it fails to offer any practical design method. In an attempt to fill this knowledge gap, a series of physical model tests of suction anchors under multi-directional loading are carried out in this study, examining loading conditions that are relevant for shared anchors. The focus is to identify the potential risks and to assess the anchor performance under shared anchoring. Based on the experiments, the following risks are identified:

- The resultant load inclination angle differs between a single line anchor and a shared anchor, leading to changes in holding capacity;
- The effects of multi-directional loading under typhoon passage influence the anchor behaviors by altering the resultant load inclination angle in essence.

The implications for design are that when performing shared suction design, the most critical resultant load inclination angle ($\alpha_{R,\ critical}$) must be carefully assessed, considering the possible worst-case scenarios, particularly during typhoon passage. $\alpha_{R,\ critical}$ is the dominant factor that governs the multi-directional loading behaviors of suction anchors. The padeye depth should be designed considering the critical load inclination angle.

5 ACKNOWLEDGEMENTS

The authors wish to gratefully acknowledge the financial support by the National Natural Science Foundation of China under Grant no. 52471273.

6 REFERENCES

Abadie, C.N. 2025. Shared Anchor Pile Response to Multi-Directional Lateral Cyclic Loading. *5th International Symposium on Frontiers in Offshore Geotechnics*, Nantes, France

Barron, J., Rouainia, M., Charlton, T., Edwards, S., & Gibson, F. 2024. Seismic performance of shared suction caisson anchors installed in liquefiable sand for floating offshore wind turbines. *Soil*

Dynamics and Earthquake Engineering, *180*, 108598. https://doi.org/https://doi.org/10.1016/j.soildyn.2024.108598

Barron, J. R., Land, E., Rouainia, M., Charlton, T. S., Hu, Z., Ng, C., & Gibson, F. 2025. The performance of shared suction caisson anchors in sand for FOWT with taut mooring. *5th International Symposium on Frontiers in Offshore Geotechnics*, Nantes, France

Chung, J. 2012. *Physical Modeling of Suction Caissons Loaded in Two Orthogonal Directions for Efficient Mooring of Offshore Wind Platforms*.

Diaz, B. D., Rasulo, M., Aubeny, C. P., Fontana, C. M., Arwade, S. R., DeGroot, D. J., & Landon, M. 2016. Multiline anchors for floating offshore wind towers. *OCEANS 2016, Shanghai.*

DNV**.** 2021. *DNV-ST-0119: Floating wind turbine structures*. Det Norske Veritas.

Finnie, I.M.S, & Randolph, M. 1994. Punch-through and liquefaction induced failure of shallow foundations on calcareous sediments. *7th International Conference on the Behaviour of Offshore Structures*.

Fontana, C., Hallowell, S., Arwade, S., DeGroot, D., Landon, M., Aubeny, C., Diaz, B., Myers, A., & Ozmutlu, S. 2018. Multiline anchor force dynamics in floating offshore wind turbines. *Wind Energy*, *21*. https://doi.org/10.1002/we.2222

Fontana, C. 2019. A Multiline Anchor Concept for Floating Offshore Wind Turbines.

Fu, D., Zhang, Y., Yan, Y., & Jostad, H. P. 2020. Effects of tension gap on the holding capacity of suction anchors. *Marine Structures*, *69*, 102679. https://doi.org/10.1016/j.marstruc.2019.102679

Herduin, M. 2019. Multi-directional loading on shared anchors for offshore renewable energy: Definition and preliminary investigation into soil behaviour and anchor performance.

Huang, L., Coughlan, K., Martinez, A., Wilson, D., Aubeny, C., Arwade, S., DeGroot, D., & Beemer, R. 2025. Centrifuge modelling of shared ring anchors for floating wind turbines subjected to cyclic loading in clay. *5th International Symposium on Frontiers in Offshore Geotechnics*, Nantes.

Li, J., Pan, S., Chen, Y., Fan, Y.-M., & Pan, Y. 2018. Numerical estimation of extreme waves and surges over the northwest Pacific Ocean. *Ocean Engineering*, *153*, 225-241. https://doi.org/https://doi.org/10.1016/j.oceaneng.2018.01.076

Li, P., Zhang, Y., Wang, Z., Teng, Y., Yi, J., Mu, T., Wu, J., & Wu, Q. 2023. Development of design typhoon profile for offshore wind turbine foundation design in Southern China. *Marine Structures*, *92*, 103479. https://doi.org/https://doi.org/10.1016/j.marstruc.2023.103479

White, D. J., Gaudin, C., Boylan, N., & Zhou, H. 2010. Interpretation of T-bar penetrometer tests at shallow embedment and in very soft soils. *Canadian Geotechnical Journal*, *47*(2), 218–229. https://doi.org/10.1139/t09-096

Yan, B., Zhu, W., Gao, B., Ye, G., Tian, Y., & Wang, Y. 2024. Bearing capacity analysis and mechanism study of shared caisson under multidirectional loading. *Ocean Engineering*, *301*, 117530. https://doi.org/10.1016/j.oceaneng.2024.117530